

Development of a new hollow cylinder apparatus

for generalised stress path testing

by Dr Brendan O'Kelly, Trinity College Dublin, and Pat Naughton, National University of Ireland, Galway.

Introduction

Accurate determination of the mechanical and pore-pressure responses of the ground to applied loads is fundamental to soil mechanics design. However, laboratory-measured stiffness values are often inconsistent with the values obtained from back-analysis of the ground performance, principally due to limitations of standard test apparatus (which have limited sample loading and boundary conditions) and sample disturbance effects. For example, the Bishop and Wesley stress path and triaxial apparatus can only subject a test specimen to axis-symmetric loading conditions.

Most ground engineering problems, however, involve multi-directional loading that invariably causes rotations of the principal stress axes and changes in the relative magnitude of the intermediate principal stress in the ground.

The more sophisticated hollow cylinder apparatus (HCA) allows independent control of the magnitude of the three principal stresses and rotation of the major-minor principal stress axes making more generalised stress path testing possible. Although such equipment is still rare, development and use has steadily increased, principally at leading research establishments (Hight et al (1983); Ampadu and Tatsuoka (1993); and Richardson et al (1996)).

A new automated HCA (Figure 1) was recently developed at the Department of Civil Engineering, University College Dublin (*Ground Engineering* April 2003). The new apparatus allows accurate measure-

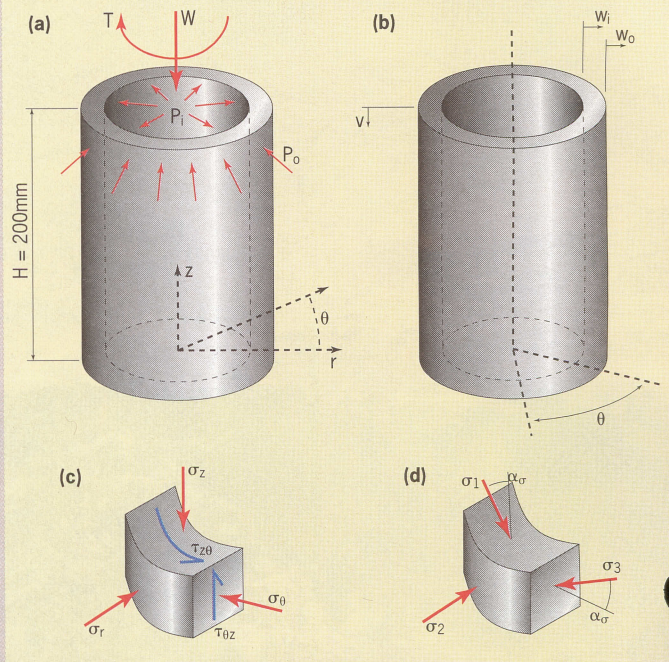


Figure 2: Stress and deformation states of hollow cylindrical sample. 2a: Applied loads and confining pressures. 2b: Sample deformations. 2c: Induced mean stresses. 2d: Resolved principal stresses.

Figure 4 (RIGHT): The sample reaction-platen assembly (O'Kelly, 2000)

ment of the mechanical and pore-pressure responses from very small strains (of the order of 10^{-5} strain) to sample failure, following generalised stress paths.

Principle of hollow cylinder testing

The apparatus tests a thick-walled hollow cylindrical sample, 100mm outer diameter, 71mm inner diameter and 200mm long (Figure 2). Hydrostatic confining pressures, p_o and p_i , are applied to the outer and inner sample walls respectively (Figure 2a). Coaxial (W) and torsional (T) loads are applied to the sample ends via annular platens. Figure 2b shows the axial (v), radial (w_o, w_i) and twist (θ) sample deformations.

Four non-zero polar stresses ($\sigma_z, \sigma_r, \sigma_\theta, \tau_{z\theta}$) are induced in an element of the sample wall (Figure 2c). The radial confining stress (σ_r) is

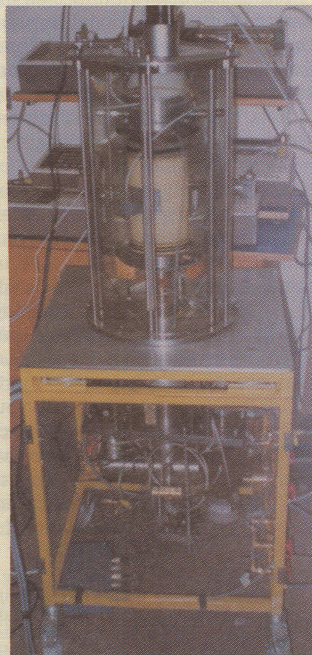


Figure 1 (LEFT): The new UCD hollow cylinder apparatus.

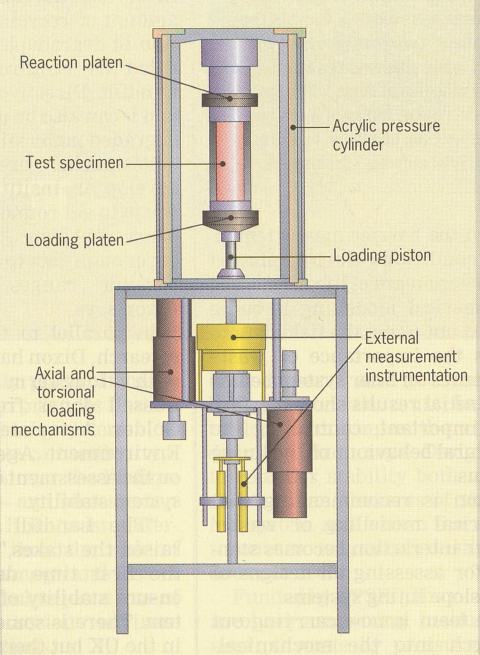
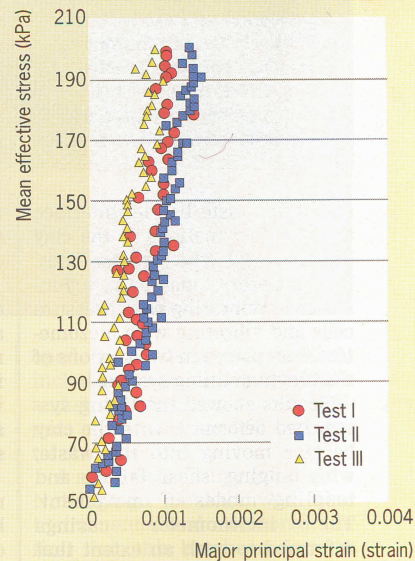
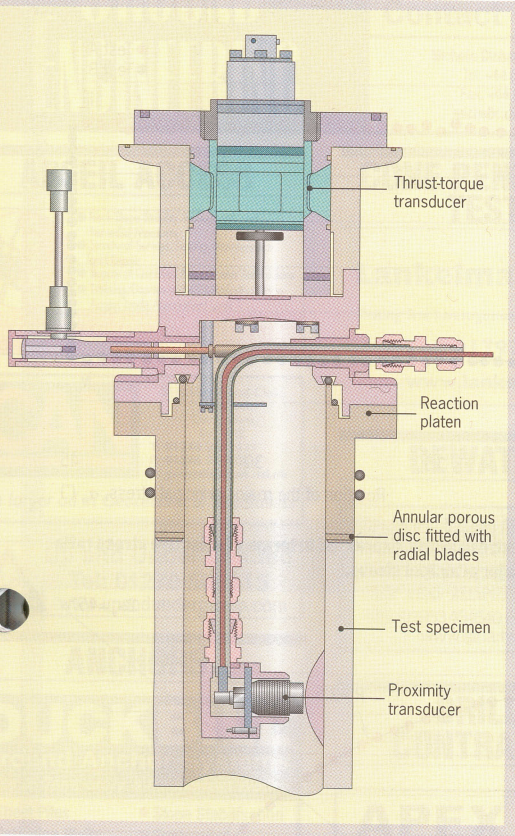


Figure 3 (RIGHT): Schematic of new UCD hollow cylinder apparatus (O'Kelly, 2000).





a principal stress, usually the intermediate principal stress. Hence, application of the torque causes rotation (α_r) of the major-minor principal stress axes in the vertical plane (Figure 2d). The magnitude and direction of the major and minor principal stresses are resolved from the four induced polar stresses using the Mohr circle of stress analysis.

Stress non-uniformity develops across the sample wall whenever a torque and/or unequal confining pressures

are applied due to the wall curvature (Wijewickreme and Vaid (1991)). An analysis of possible sample geometries indicated that the selected sample size would result in reasonably homogeneous stress distributions acting across the sample wall for generalised stress conditions.

The University College Dublin hollow cylinder apparatus
Cell loading mechanisms and pressure systems

Figure 3 shows the general arrangement of the new hollow cylinder apparatus. The traditional HCA layout was rearranged so the new apparatus is more compact and the pressure cell is more easily assembled and dismantled.

The sample ends are in contact with two annular platens inside the

cell, 340mm diameter by 600mm high, and the sample is enclosed between outer and inner rubber membranes. The outer cell chamber and the inner bore cavity of the sample are independently sealed.

Digital pressure-volume controllers (from GDS Instruments) independently control the confining pressures (applied to the cell chamber and bore cavity) and the back-pressure (applied to the sample base). The cell tie bars, connecting the cell top and base plates, are located inside the acrylic pressure cylinder.

Axial and twist boundary displacements are applied to the base of the sample – which is restrained at its upper end – via the 25mm diameter loading piston. Eight thin, radial blades protruding above the rough porous discs, which are fastened to the annular platens, ensure full torque transmission to the sample ends.

Innovative mechanisms to displace and rotate the loading piston, which passes through the cell base, are secured to the reaction frame located beneath the cell. Screw and spline type bearings, integrated about the lower end of the piston, facilitate smooth vertical, rotary and spiral piston motions.

Rated axial and torsional working loads of 19.3kN and 103Nm (corresponding to unconfined compressive and torsional shear stresses of 5MPa and 0.6MPa respectively) can be applied to the sample. The working stress domain allows generalised stress path testing, to failure, of all geomaterials including soft to weak rock.

Axial and rotary slack (when the loading directions are reversed) in the mechanisms is limited to 1 μ m and 15 arc-seconds respectively. This stiffness permits accurate cyclic and dynamic testing.

Instrumentation and automation

The new HCA is automatically closed-loop controlled to permit generalised stress path testing. The GDS controllers independently measure and control the applied confining pressures and volume changes of the outer cell and inner bore chambers and the test specimen. A differential pressure transducer also measures the effective sample confining pressure.

Instruments inside the pressure cell measure the axial and torsional loads (developed across the sample length) and the sample deformational response.

The loads are measured using a combined thrust-torque transducer incorporated in the sample reaction platen (Figure 4). Three Imperial College inclinometer gauges (Symes and Burland (1984)), which were modified to the authors' design, and two proximity transducers measure sample strains over the middle third of the sample length to resolutions of better than 5x10⁻⁵ strain.

Deformations are measured locally to exclude errors due to apparatus compliance and sample end-restraint and bedding effects. The inclinometer gauges are attached to the outer sample membrane and measure axial and twist deformations of the sample. Proximity transducers located in the outer cell and inner bore chambers measure radial displacements of the sample wall.

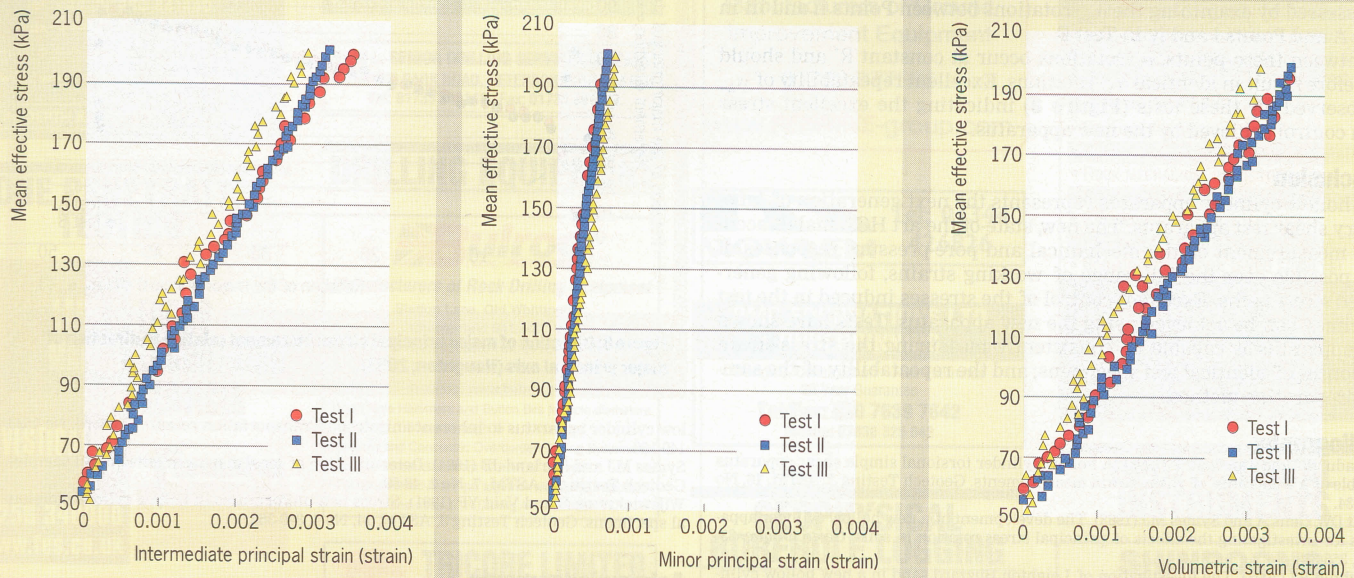


Figure 5: Stress-strain responses of isotropically consolidated test specimens in terms of (a) major (b) intermediate (c) minor principal strains and (d) volumetric strain (Naughton, 2003).

Backup measurements from outside the cell are provided by two displacement transducers and a rotary encoder which measure piston movements and hence the axial and twist sample boundary displacements. Special calibration procedures, which improve the instrument accuracy relative to that achieved by other apparatus, were developed. For example, the proximity transducers are calibrated using an optical table and laser measurement system.

Stepper motors drive the mechanisms that apply the axial and twist boundary displacements to the sample ends. A suite of LabVIEW programs interface with the motors, the GDS pressure-volume controllers and the instruments to control the four induced sample stresses (σ_z , σ_r , σ_θ , $\tau_{z\theta}$) to within 0.5kPa of the targeted values. Algorithms were developed to enhance the pressure resolution of the standard GDS controllers.

Axial and twist sample boundary displacements are applied in 0.1 μ m and 0.8 arc-second steps (or strain resolutions of better than 10⁻⁶ strain) by the loading mechanisms. The control programs continuously compute the stress state and the sample strain response from the load-pressure-deformation instrument readings. A prescribed generalised stress path is followed by sequentially moving between transitional target stress points located along the stress path. The program commands the stepper motors and controllers to simultaneously adjust the sample stresses to arrive at the next stress point on the stress path, and the process is repeated.

Results of proving tests

The test capabilities of the new apparatus were investigated by asking it to follow both isotropic and anisotropic stress paths. Identical test specimens of medium-to-dense Leighton Buzzard sand were subjected to isotropic stress paths that increased the mean effective stress in the samples from 50kPa to 200kPa. Good repeatability of the principal and volumetric strains was achieved (Figure 5) indicating both the reliability of the sample preparation method and the capability of the apparatus to record consistent stress-strain responses.

Anisotropic stress paths, where the stress state of identical sand test specimens was changed along two different stress paths, are presented (Figure 6). The stress paths involved anisotropic consolidation (quantified in terms of the effective stress ratio (R') the ratio of the major to minor effective principal stresses) and rotation (α_σ) of the major principal stress direction. The actual mean induced stresses deviated by less than $\pm 2.5\%$ from their target values for these stress paths.

A plot of torsional shear stress ($\tau_{z\theta}$) versus normal stress difference ($(\sigma_z - \sigma_\theta)/2$) is a useful method to describe the rotation of the principal stress axes. When plotted to the same scale, constant values of R' appear as quadrants centred on the origin, with α_σ represented by lines radiating from the origin.

The stress changes between two points along these stress paths define the rotation of the major principal stress increment direction ($\alpha_{\Delta\sigma}$). The stress paths for Tests A and B, during α_σ rotation at constant R', describe circular paths (Figure 7).

The capability of the apparatus to follow a predefined stress path can be assessed by examining the $\alpha_{\Delta\sigma}$ rotations between Points ii and iii in Test A and Points i and iv in Test B.

Between these points, α_σ rotations occur at constant R' and should therefore result in identical $\alpha_{\Delta\sigma}$ rotations. Excellent repeatability of $\alpha_{\Delta\sigma}$ is observed for these tests (Figure 8) indicating the excellent stress path control achieved by the new apparatus.

Conclusion

The hollow cylinder apparatus represents the next generation of laboratory shear test apparatus. The new, state-of-the-art HCA makes accurate measurement of the mechanical and pore-pressure responses of soil possible over the full range of working strains, following generalised stress paths. Excellent control of the stresses induced in the test specimen can be achieved using the new apparatus. Tests have shown the apparatus is capable of consistently measuring the stress-strain responses of identical test specimens; and the repeatability of the sample preparation method.

Bibliography

- Ampadu, SK and Tatsuoka F (1993). A hollow cylinder torsional simple shear apparatus capable of a wide range of shear strain measurements. *Geotech Testing J, ASTM*, 16, No 1, 14-34.
- Hight DW, Gens A and Symes MJ (1983). The development of a new hollow cylinder apparatus for investigating the effects of principal stress rotation in soils. *Géotechnique*, 33, No 4, 355-383.
- Naughton PJ (2003). The investigation of Leighton Buzzard sand in a new hollow cylinder apparatus. PhD thesis, submitted to University College Dublin.
- O'Kelly BC (2000). Development of a new apparatus for hollow cylinder testing. PhD Thesis, University College Dublin.
- Richardson IR, Chapman DN and Brown S (1996). Relating failure tests performed in hol-

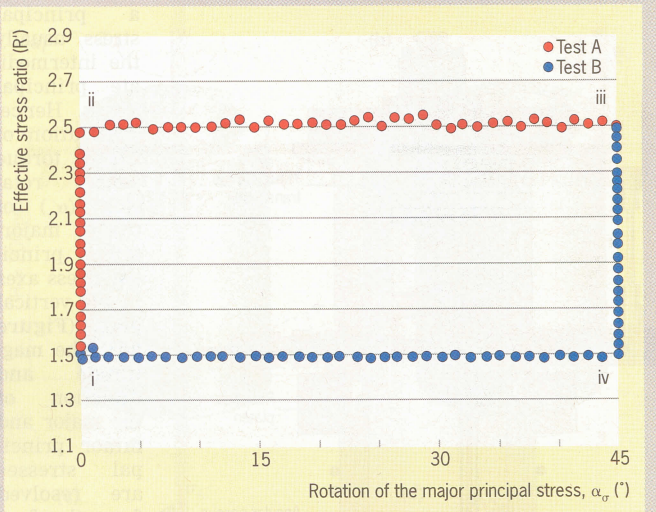


Figure 6: Anisotropic stress paths, expressed in terms of effective stress ratio and rotation of the major principal stress.

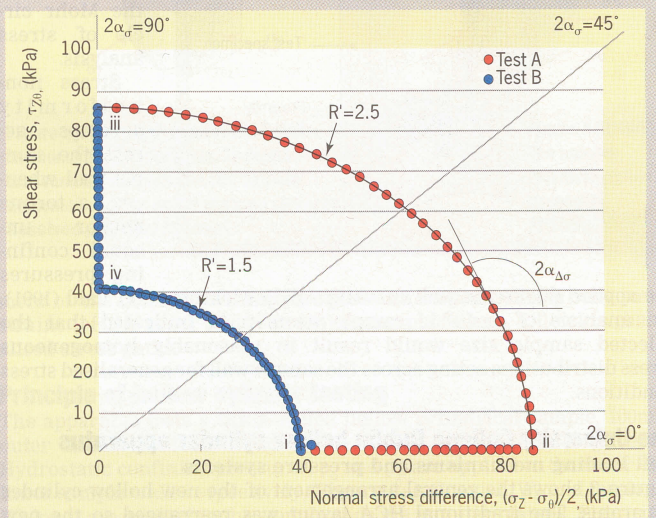


Figure 7: Torsional shear stress to normal stress difference for the proving tests (Naughton, 2003).

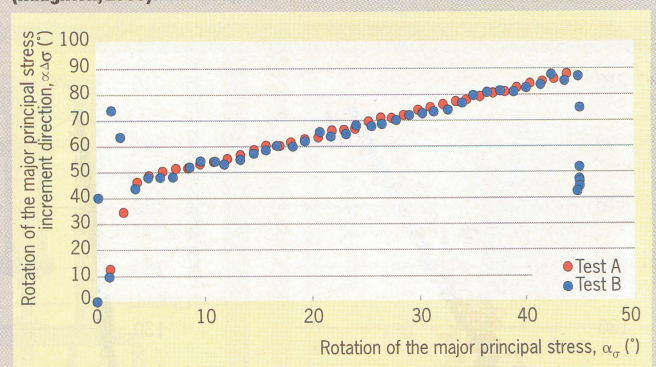


Figure 8: Direction of major principal stress increment relative to direction of major principal axis (Naughton, 2003).

low cylinder apparatus to inherent anisotropy. Transportation research record, No 1526, 149-156.
 Symes MJ and Burland JB (1984). Determination of local displacements on soil samples. *Geotech Testing J, ASTM*, 7, No 2, 49-59.
 Wijewickreme D and Vaid YP (1991). Stress non-uniformities in hollow cylinder torsional specimens. *Geotech Testing J, ASTM*, 14, No 4, 349-362.

Acknowledgements

The authors would like to thank Dr Tom Widdis for his support during this research project and Dr Trevor Orr for his helpful comments during the preparation of this article.